J Therm Anal Calorim (2012) 110:661–669
DOI 10.1007/s10973-011-1890-1

Thermal decomposition of Prussian blue under inert atmosphere

Claudia Aparicio · Libor Machala · Zdenek Marusak

Received: 21 June 2011 / Accepted: 25 August 2011 / Published online: 14 September 2011

Abstract The thermal decomposition of Prussian blue (iron(III) hexacyanoferrate) under inert atmosphere of argon was monitored by thermal analysis from room temperature up to 1000 °C. X-ray powder diffraction and ^{57}Fe Mössbauer spectroscopy were the techniques used for phase identification before and after sample heating. The decomposition reaction is based on a successive release of cyanide groups from the Prussian blue structure. Three principal stages were observed including dehydration, change of crystal structure of Prussian blue, and its decomposition. At 400 °C, a monoclinic Prussian blue analogue was identified, while at higher temperatures the formation of various polymorphs of iron carbides was observed, including an orthorhombic Fe_2C. Increase in the temperature above 700 °C induced decomposition of primarily formed Fe_7C_3 and Fe_2C iron carbides into cementite, metallic iron, and graphite. The overall decomposition reaction can be expressed as follows: $Fe_4[Fe(CN)_6]_3 \cdot 4H_2O \rightarrow 4Fe + Fe_3C + 7C + 5(CN)_2 + 4N_2 + 4H_2O$.

Keywords Insoluble Prussian blue · Iron carbide · XRD · Calcination

Electronic supplementary material The online version of this article (doi:10.1007/s10973-011-1890-1) contains supplementary material, which is available to authorized users.

C. Aparicio · L. Machala (✉) · Z. Marusak
Regional Centre of Advanced Technologies and Materials, Departments of Experimental Physics and Physical Chemistry, Faculty of Science, Palacky University, Slechtitelu 11, 783 71 Olomouc, Czech Republic
e-mail: libor.machala@upol.cz
URL: http://www.rcptm.com/

Introduction

The Prussian blue (PB) complex salt was unwittingly produced by a painter in the beginning of the eighteen century. From this day until now, PB has been employed in a wide range of applications in industry, pharmaceutics, and science. Prussian blue, "insoluble" PB, iron(III) hexacyanoferrate or ferric ferrocyanide are usually the names of this ferrocyanide compound. PB has an ideal chemical formula of $Fe_4^{III}[Fe^{II}(CN)_6]_3 \cdot xH_2O$ with the Fm-3m space group [1], where Fe^{2+} ions are found in a low-spin ($S = 0$) state and Fe^{3+} ions are found in a high-spin ($S = 5/2$) state. PB shows a ferromagnetic behavior below its Curie temperature $T_C = (5.5 \pm 0.5)$ K [2].

Physicochemical properties of PB have been investigated by several experimental techniques including infrared spectroscopy [3], X-ray diffraction [4], and Mössbauer spectroscopy (MS) [2, 6, 7]. These investigations were devoted to structural analysis [1, 8, 9], synthesis [10–12], magnetic properties [13], applications [14–16], PB-based analogs [17, 18], and some of them have been focused on behavior of PB at high temperatures [5, 6, 19].

In general, when hexacyanoferrate compounds containing crystalline water are heated, one endothermic effect (always below 200 °C) corresponds to a release of the water molecules. Afterward, the thermal decomposition occurs at higher temperatures depending on the composition of the starting compound [20]. According to De Marco [20–23], Brar [24], and Lehto [25] the decomposition of hexacyanoferrate compounds in air occurs with an exothermic effect and accompanied by a release of gaseous products ($(CN)_2$ or HCN). Finally, the oxidation of iron cations leads to the formation of iron oxides as common decomposition products [19, 24–27].

One of the oldest works on thermal decomposition of hexacyanoferrate in vacuum was reported by Gallagher and Prescott [28]. They studied thermal decomposition reactions of europium hexacyanoferrate(III) and ammonium europium hexacyanoferrate(II) compounds resulting to Eu hydroxide and $Fe(CN)_2$. Further decomposition of $Fe(CN)_2$ to Fe_3C and finally to metallic iron has been confirmed. Cosgrove et al. [18] studied thermal behavior of Prussian blue up to 530 °C in vacuum and in air using thermal analysis, X-ray diffraction, and MS. According to Mössbauer spectra, they identified the changes in iron sites with a temperature before and after cyanide release taking place around 290 °C. The reversibility of the process was proved only if the sample was heated at temperatures below 450 °C. Finally, the authors concluded that the structure of PB heated in vacuum up to 450 °C was partially destroyed and crystalline ferrous ferrocyanide with undetermined crystal structure was formed. On the other hand, when the PB sample was heated in air at 410 °C they obtained magnetite in addition to the above-mentioned phases.

Other study on PB thermal decomposition carried out in argon [5] described the simple mechanism toward Fe_3C, graphite and nitrogen as the final products. Years later, Inoue et al. [6] published the Mössbauer characterization of thermal decomposition products of PB in vacuum. In this paper, Inoue et al. explained the thermal behavior of the dried PB from 200 to 350 °C and assumed that changes in Mössbauer parameters above 250 °C corresponded to a flipping of cyanoligands or an existence of mixed-valence states. Therefore, it is clear that a full decomposition of PB has not been achieved at such low temperatures. Thus, one can see from the literature overview that the behavior of PB at high temperatures is not still completely understood. In order to fill this knowledge gap, this study is focused to describe the thermal behavior and elucidate the decomposition mechanism of PB at temperatures up to 1000 °C under an inert atmosphere.

Materials and methods

Starting material and sample preparation

The insoluble Prussian blue ($Fe_4[Fe(CN)_6]_3{\cdot}xH_2O$) nanoparticles (60–80 nm) used in this study were manufactured by Sigma Aldrich. The Prussian blue nanopowder (PB) was heated up to different temperatures in argon atmosphere (gas flow of 30 mL/min, protective gas flow of 10 mL/min (Ar)), inside of an opened alumina crucible. The heating rate was 10 °C/min and the mean mass of the samples was 16 mg. The heat treatments of the samples were performed using a thermal analyzer (STA 449 C Jupiter, Netzsch) enabling simultaneous thermogravimetric analysis (TG) and differential scanning calorimetry (DSC). The analyzer is coupled to mass spectrometer (QMS 403 Aëolos, Netzsch) for the analysis of evolving gases (EGA) during the decomposition reaction. The PB was heated up to following temperatures: 400, 670, and 1000 °C. They were labeled as PB1, PB2, and PB3, respectively.

Samples characterization

All the samples were characterized by X-ray powder diffraction (XRD) and transmission ^{57}Fe MS. XRD patterns were recorded with a PANalytical X'Pert PRO MPD diffractometer (Co Kα radiation) in the Bragg–Brentano geometry, equipped with an X′Celerator detector and programmable divergence and diffracted beam anti-scatter slits. The samples were placed on a zero-background Si slide, gently pressed and scanned with a step size of 0.017°, and with angular range from 10° to 90°. The identification of crystalline phases in the recorded XRD patterns was performed using the High Score Plus software (PANalytical) in conjunction with PDF-4+ database.

Transmission ^{57}Fe MS (1024 channels) was carried out in a constant acceleration mode using a ^{57}Co gamma source in Rh matrix at room temperature (RT). The spectrometer was calibrated with a α-Fe foil, and the isomer shift (IS) values were expressed with respect to metallic α-iron at room temperature. The spectra were folded and fitted by Lorentz functions using the computer program CONFIT2000 [29]. Relative contents of iron-bearing phases are expressed through atomic percents given from a relative area of a given subspectrum.

Results and discussion

Characterization of PB samples

The PB sample was characterized by XRD and ^{57}Fe MS. Both techniques proved that the initial Prussian blue sample contained an admixture of a minor phase (~3%) identified as mineral jarosite ($(K,Na)Fe_3(SO_4)_2(OH)_6$). The Mössbauer spectrum was fitted with two doublets and one singlet (Fig. 1). The singlet and the major doublet correspond to low-spin (LS) ferrous ions octahedrally coordinated to six C atoms (IS = −0.14 mm/s, 50.6%) and high-spin (HS) ferric ions octahedrally coordinated to six N atoms (IS = 0.41 mm/s, QS = 0.17 mm/s, 47.0%) in Prussian blue, respectively. The minor doublet corresponds to ferric ions (IS = 0.32 mm/s, QS = 1.13 mm/s, 2.4%) in octahedral site of jarosite [30].

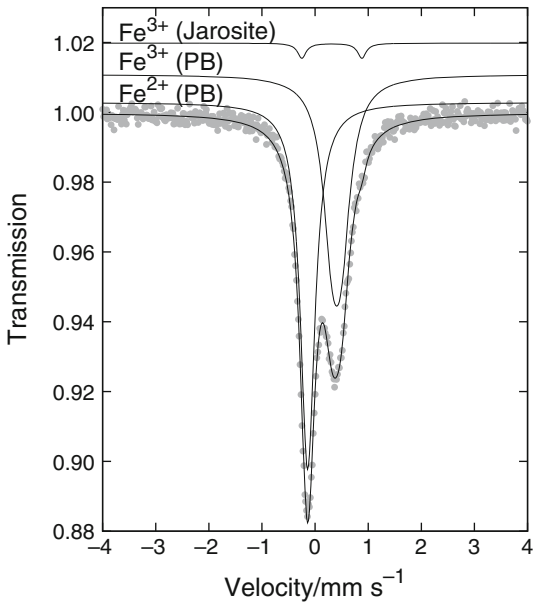

Fig. 1 RT Mössbauer spectrum of the PB sample. The subspectra are shifted along the vertical axis for clarity

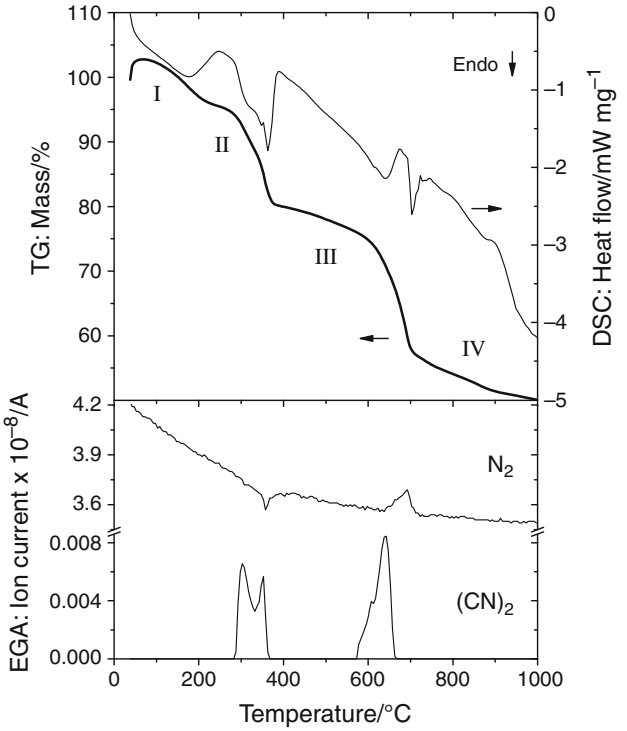

Fig. 2 TG (*thick black line*), DSC (*thin black line*), and EGA (*lower part*) of the PB sample carried out in argon atmosphere. *Roman numbers* indicate the stages of decomposition

Thermal behavior of PB

Simultaneous TG and DSC analyses under argon atmosphere up to 1000 °C (Fig. 2) showed four decomposition steps: I (67–262 °C), II (262–377 °C), III (377–707 °C), and IV (707–1000 °C). In step I, the mass decrease (7.62%) was assigned to water loss from the PB structure, accompanied by an endothermic peak at 178 °C in DSC graph and a wide peak with a centroid at 210 °C in the evolved gas analysis graph (not displayed). The number of water molecules per one molecule of PB was determined as four from TG. The mass losses detected within the steps II (14.75%) and III (23.02%) correspond mainly to a release of cyanide groups from the PB structure at average temperatures of 308, 352, 608, and 643 °C (Fig. 2), accompanied by endothermic reactions (I: 318 and 348 °C, II: 613 and 643 °C). In step III, in addition to $(CN)_2$ emission a release of nitrogen at 693 °C accompanied by an endothermic reaction has been detected. On the other hand, a consumption of nitrogen represented by a downward peak at 358 °C can not be related to the decomposition reaction but it only indicates the detection of other new formed gas by the mass spectrometer, which for a moment changes relative concentrations of the gases. Moreover, an irregular release of carbon dioxide, which was probably adsorbed from air by the surface of the PB sample before the measurement of thermal analysis, was detected by EGA (not displayed) within the measurement.

Sample heated up to 400 °C

The thermal analysis finished at 400 °C (sample PB1) shows that the original structure of PB released all of its structural water ($4H_2O$) and six $(CN)^-$ groups, i.e., $3(CN)_2$ in gaseous form (cyanogen). Temperature of crystal water release (210 °C) agrees well with other thermal studies of PB and PB analogs [5, 18].

The evident change in PB structure has been observed in both XRD pattern (Fig. 3) and Mössbauer spectrum (Fig. 4a) of PB2 ("as-prepared" sample), however, the spectral components of the original PB (~25%) are still present. Unfortunately, it was not possible to find any pattern in the PDF-4+ database, which matches the diffraction lines of the newly formed phase (Fig. 3). Given that some of these compounds are unstable, the same sample was characterized again after one and half year ("aged" sample) to verify its stability. This new XRD pattern is slightly different from the "as-prepared" PB2 sample. The cell group and cell parameters of those unknown phases were calculated with Fullprof 2000 software [31]. It was found that both phases show a monoclinic structure with space group P 2/m, nevertheless a difference in the cell parameters confirms the instability of the structure (see figures S1 and S2 on supporting information).

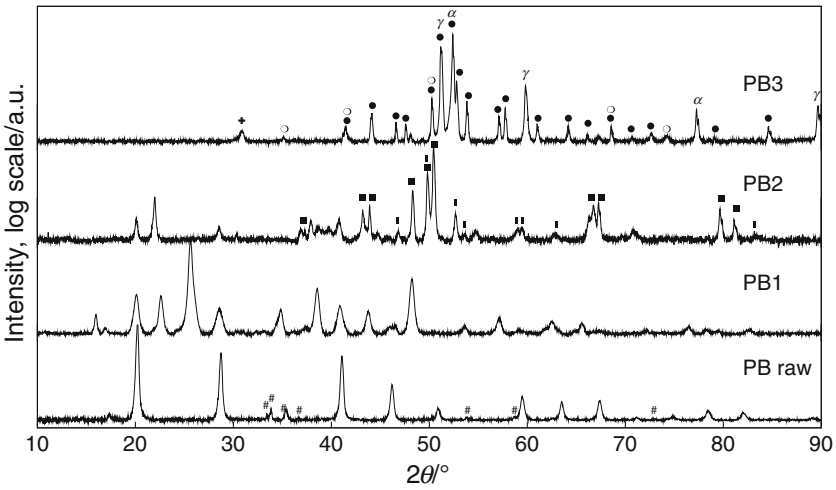

Fig. 3 XRD patterns of the PB samples before and after thermal analyses carried out in inert atmosphere. The *symbols* in the graphs represent the identified phases: Jarosite (#), Fe_2C (*filled square*), Fe_7C_3 (*vertical bar*), Fe_3C (*filled circle*), alpha iron (α), gamma iron (γ), magnetite (*open circle*), and graphite (*plus symbol*). Samples heated up to: 400 °C (PB1), 670 °C (PB2), and 1000 °C (PB3)

RT Mössbauer spectrum of PB2 consists of six spectral components (Fig. 4a), of which the singlet L1 and one doublet D1 belong to the starting PB (Table 1a). The increase in the quadrupole splitting (QS) value of D1 doublet agrees with the change in the environment of Fe^{3+} (HS) due to a dehydration process in Prussian blue [6]. D2 doublet has typical values for LS ferric iron octahedrally coordinated to six carbon atoms in $M_3[Fe(CN)_6]_2$ structures [32]. D3 doublet has the IS and QS values very close to those for Fe^{2+} HS in $K_2Fe[Fe(CN)_6]$ (IS = 1.09 mm/s, QS = 0.45 mm/s) [33]; a doublet with similar values of IS and QS were also obtained from pyrolyzed soluble Prussian blue ($FeK[Fe(CN)_6]\cdot xH_2O$), and aged Prussian brown ($Fe(H_3O)[Fe(CN)_6]\cdot xH_2O$). Mössbauer parameters of D4 and D5 doublets are comparable with those of ferrous trivalent hexacyanides ($Fe_3[M^{III}(CN)_6]_2\cdot xH_2O$), which have a cubic structure and two different iron environments [34].

The doublets D2 and D4 show hyperfine values corresponding to flipping of cyano ligands in PB structure as proposed by Inoue et al. [6]. In our case this indicates the change in the crystal structure of PB after the beginning of its decomposition. Our Mössbauer spectrum resembles the spectrum measured on a PB sample heated up to 460 °C in a vacuum by Cosgrove et al. [18]. They suggest the formation of ferrous ferricyanide after heating when PB has released cyanide groups. Ferrous ferricyanide is not a stable compound; therefore the newly formed compound may be a different one with no cubic structure. With respect to the IS values, the doublets D2 and D3 correspond to iron atoms octahedrally coordinated with six carbon and nitrogen atoms, respectively. From relative areas of subspectra, it is possible to determine the relation between ferric and ferrous ions as $Fe^{3+}/Fe^{2+} = 0.89$. Thus, a possible arrangement of iron atoms can be expressed as $Fe^{+2}_{1.2}Fe^{+2}_{1.8}[Fe^{+3}(CN)_6]_2$, where LS Fe^{3+} is identified by D2 component, and HS Fe^{2+} is identified by D3, D4, and D5 subspectra.

The Mössbauer measurement of the aged PB1 sample (Fig. 4b; Table 1b) also revealed that the structure did not remain stable. The change is reflected by an absence of D4 and D5 doublets, but a presence of a new doublet with the hyperfine parameters typical for a mixed-valence state and the second singlet with the IS peculiar to low-spin ferrous ions. The aging process is thus based on a slow oxidation of the sample.

Sample heated up to 670 °C

Three crystalline phases including Prussian blue, Eckström-Adcock carbide (Fe_7C_3, space group $P6_3mc$) and iron carbide (Fe_2C) have been identified by XRD (Fig. 3). The latter phase is predominant and the corresponding diffraction lines match for two patterns in the database, the first one is a pseudo-hexagonal ε'-Fe_2C and the second one is an orthorhombic Fe_2N. Nevertheless, there are still a few more diffraction lines in the diffractogram that could not be assigned to any pattern in the database.

The very complex RT Mössbauer spectrum of PB2 sample was fitted by five sextets, three doublets, and one singlet (Fig. 5, Table 2). S1, S2, and S3 sextets were ascribed to three non-equivalent positions of iron atoms in the hexagonal structure of Fe_7C_3 (sum of sub-spectral areas: 10.3%) [35]. Literature values for the hyperfine interactions of Fe_7C_3 were taken from Lodya's and Yamada's papers [36, 37]. L1 singlet and D3 doublet show the hyperfine parameters typical for anhydrous Prussian blue. Relatively low areas of L1 and D3 subspectra (together 11.6%) point out that decomposition of the Prussian blue is almost completed at this temperature (670 °C).

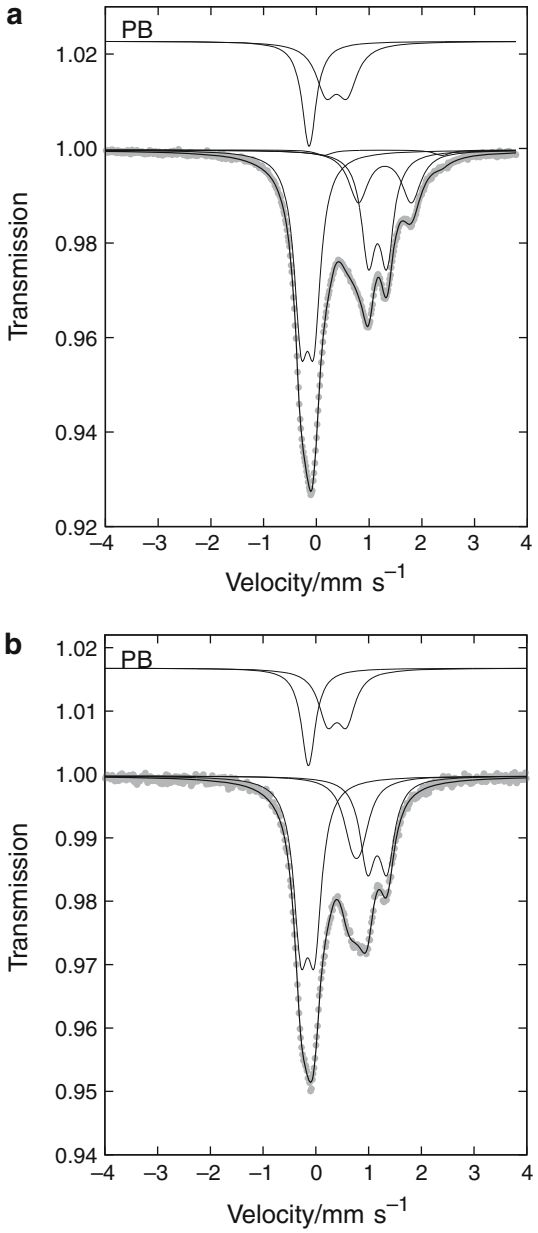

Fig. 4 RT Mössbauer spectra of PB1 (400 °C): **a** "as-prepared" and **b** aged. The subspectra are shifted along the vertical axis for clarity

Table 1 Mössbauer parameters of the PB1 sample (400 °C): a) "as-prepared" and b) aged

	Iron state	IS[a]/mm s^{-1}	QS/mm s^{-1}	W/mm s^{-1}	Area/%
(a)					
D1	Fe^{3+} HS	0.38	0.40	0.47	14.7
D2	Fe^{3+} LS	−0.17	0.24	0.32	34.6
D3	Fe^{2+} HS	1.16	0.35	0.32	22.4
D4	Fe^{2+} HS	1.30	1.00	0.44	15.3
D5	Fe^{2+} HS	1.26	2.24	0.37	1.4
L1	Fe^{2+} LS	−0.14	–	0.32	11.6
(b)					
D1	Fe^{3+} HS	0.40	0.36	0.41	14.9
D2	Fe^{3+} LS	−0.16	0.26	0.32	36.4
D3	Fe^{2+} HS	1.16	0.36	0.35	22.0
D4	$Fe^{2+/3+}$ HS	0.77	0.16	0.42	14.9
L1	Fe^{2+} LS	−0.14	–	0.32	11.8

IS isomer shift (±0.01), *QS* quadrupole splitting (±0.01), *W* experimental line width (±0.01), Area (±0.5), *D* doublet, *L* singlet, *HS* high spin, *LS* low spin

[a] Relative to metallic iron (α-Fe)

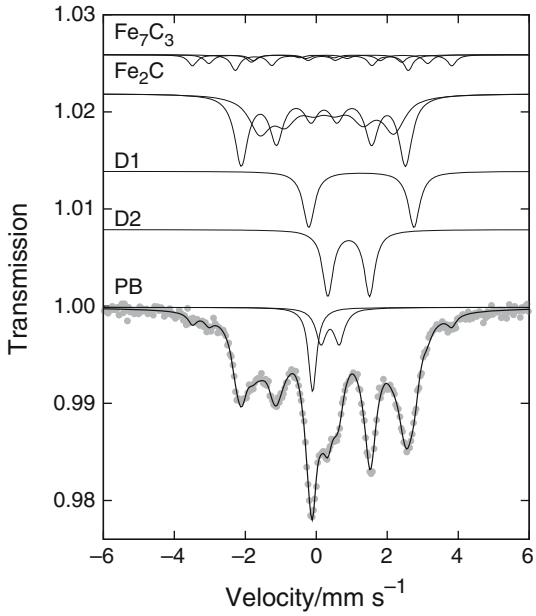

Fig. 5 RT Mössbauer spectrum of sample PB2 (670 °C). The subspectra are shifted along the vertical axis for clarity

Sextets S4 and S5 (Fig. 5; Table 2) can be attributed to a major Fe_2C compound, which could have pseudo-hexagonal or orthorhombic structure (sum of sub-spectral areas: 56%). Although it is known that hexagonal iron carbides and iron-nitrides are isostructural [38], the orthorhombic ζ-Fe_2C (Pbcn space group) is almost unknown being in many cases incorrectly identified as pseudo-hexagonal ε′ phase [39–42]. Comparing the hyperfine parameters with those reported for Fe_2C, we can find a slight disagreement in the values of the hyperfine magnetic field. The values obtained in our work (14.4 and 11.7 T) are smaller than those usually measured for hexagonal ε-carbides (between 17 and 24 T). The lowest hyperfine magnetic field of 17 T has been obtained by Niemantsverdriet et al. [40] and Amelse et al. [41]. The reason for a smaller hyperfine field given by Le Caër et al. [42] is an alternative ordering of iron and carbon atoms in the structure or a different crystalline symmetry. Niemantsverdriet et al. [40] also measured the XRD pattern of this carbide, and they obtained

Table 2 Mössbauer parameters of sample PB2 (670 °C)

	Phase	IS[a]/mm s^{-1}	QS/mm s^{-1}	W/mm s^{-1}	B/T	Area/%
S1	Fe_7C_3	0.23	−0.13	0.30[b]	22.7	3.2
S2	Fe_7C_3	0.04	0.04	0.30[b]	19.2	2.6
S3	Fe_7C_3	0.16	0.00	0.30[b]	15.1	4.5
S4	Fe_2C	0.21	-0.02	0.45	14.4	30.5
S5	Fe_2C	0.26	0.08	0.73	11.7	25.5
D1	Fe^{2+}	1.27	2.96	0.39	–	10.7
D2	Fe^{2+}	0.91	1.18	0.36	–	11.4
D3	PB	0.39	0.52	0.36	–	5.9
L1	PB	−0.10	–	0.27	–	5.7

IS isomer shift (±0.01), *QS* quadrupole splitting (±0.01), *W* experimental line width (±0.01), *B* hyperfine magnetic field (±0.1), Area (±0.5), *S* sextet, *D* doublet, *L* singlet

[a] Relative to metallic iron (α-Fe)

[b] Fixed value

practically the same diffractogram as described by Barton and Gale [39], and which is also shown in our work (Fig. 3, sample PB2). Thus, both S4 and S5 sextets can be ascribed to an orthorhombic ζ-Fe_2C. The broader lines and smaller hyperfine field of these sextets indicate some kind of a size distribution of the iron carbide particles.

The doublets D1 and D2 could not be directly assigned to any phase. They might be a result of the formation of other phases, or they could belong to a cyanide compound of the type $Fe^{II}_3[M^{III}(CN)_6]_2$.

Sample heated up to 1000 °C

Metallic iron with bcc and fcc lattice (α and γ, respectively), cementite θ-Fe_3C (orthorhombic, Pnma space group), graphite (hexagonal, $P6_3mc$ space group) and a small amount of magnetite Fe_3O_4 (∼4 wt%), were the phases identified by XRD on sample PB3. The quantitative results obtained by Rietveld refinement of the respective XRD pattern are shown in Table 3. The aforementioned phases, except carbon, were also identified by MS; furthermore it was possible to reveal by MS that the gamma iron phase is not pure metallic iron, but fcc iron with carbon structural inclusions, i.e., austenite phase, as has been clearly indicated by the presence of a doublet subspectrum with IS close to zero (Fig. 6; Table 4). The estimation of a content of carbon atoms in the structure (0.93 wt%) was calculated according to the relationship given by Ron [43]. Magnetite identified by XRD and MS appears owing to an oxidation of metallic iron.

Table 3 Results of Rietveld refinement for the PB3 sample (1000 °C)

Phase	Weight percentage/%
α-Fe	22.8 (1)
γ-Fe	26.3 (1)
Fe_3C	38.3 (2)
Fe_3O_4	3.9 (1)
C	8.7 (3)

The number in parentheses denotes the uncertainty of the last digit ($\chi^2 = 2.52$)

Overall mechanism of thermal decomposition

Within the first step, four water molecules are released from the crystal structure of PB:

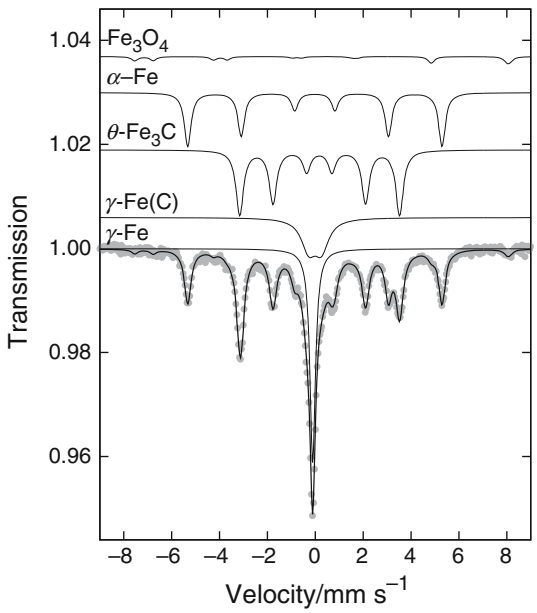

Fig. 6 RT Mössbauer spectrum of sample PB3 (1000 °C). The subspectra are shifted along the vertical axis for clarity

Table 4 Mössbauer parameters of the PB3 sample (1000 °C)

Component	IS[a]/mm s^{-1}	QS/mm s^{-1}	W/mm s^{-1}	B/T	Area/%
α-Fe	−0.02	0.00	0.34	33.0	26.3
θ-Fe_3C	0.17	0.02	0.37	20.7	35.2
Fe_3O_4 (tet)	0.29	0.01[b]	0.32[b]	48.7	1.9
Fe_3O_4 (oct)	0.61	0.02[b]	0.31[b]	45.9	1.8
γ-Fe(C)	−0.01	0.54	0.73	–	14.8
γ-Fe	−0.11	–	0.28	–	19.9

IS isomer shift (±0.01), *QS* quadrupole splitting (±0.01), *W* experimental line width (±0.01), *B* hyperfine magnetic field (±0.1), Area (±0.5)

[a] Relative to metallic iron (α-Fe)

[b] Fixed value

$$67-262\,^{\circ}\mathrm{C}:\ \mathrm{Fe_4[Fe(CN)_6]_3\cdot 4H_2O} \rightarrow \mathrm{Fe_4[Fe(CN)_6]_3} + 4\mathrm{H_2O} \quad (1)$$

The second decomposition step is accompanied by a formation of a ferricyanide phase, which could not be found in the PDF database. According to the model constructed from the analysis of the Mössbauer spectrum of the PB1 sample, it is possible to suggest the following equation:

$$67-377\,^{\circ}\mathrm{C}:\mathrm{Fe_4[Fe(CN)_6]_3\cdot 4H_2O} \rightarrow 0.26\mathrm{Fe_4[Fe(CN)_6]_3} + 0.74(7/5\ \mathrm{Fe_3^{II}[Fe^{III}(CN)_6]_2} + 3/5\ (\mathrm{CN})_2) + 4\mathrm{H_2O} \quad (2)$$

This equation, expecting the formation of the ferricyanide compound with three structural positions of high-spin ferrous ions, however, does not satisfy the mass loss determined from TG and emission of three moles of $(CN)_2$ as determined from EGA. In fact, the mass loss calculated from this reaction is only 9.1%.

In accordance with the overall mass loss of 45.39% determined from TG during the steps I, II, and III (from 67 to 707 °C), a release of 4 mol of H_2O, 4 mol of N_2, and 5 mol of $(CN)_2$ by the decomposition of 1 mol of PB can be considered (see Eq. 3). The theoretical mass loss is then $\Delta m_{th} = 47.7\%$. Importantly, while the emission of 3 mol of $(CN)_2$ during the step II results only to the structural change of the PB compound, the release of next 2 mol of $(CN)_2$ during the step III is accompanied by a total decomposition of PB toward iron carbides and graphite. Taking into account the Mössbauer spectral areas of Fe_7C_3 and Fe_2C (Table 2), we can calculate corresponding coefficients for solid decomposition products in Eq. 3.

$$67-707\,^{\circ}\mathrm{C}:\ \mathrm{Fe_4[Fe(CN)_6]_3\cdot 4H_2O} \rightarrow 3\mathrm{Fe_2C} + 1/7\ \mathrm{Fe_7C_3} + 32/7\ \mathrm{C} + 5(\mathrm{CN})_2 + 4\mathrm{N_2} + 4\mathrm{H_2O} \quad (3)$$

Within the step IV (from 707 to 1000 °C), the solid-state decompositions of Eckström-Adcock carbide (Fe_7C_3) as well as Fe_2C carbide to Fe_3C carbide (cementite) and graphite take place (Eckstrom and Adcock [44], Cohn and Hofer [45]):

$$3\mathrm{Fe_7C_3} \rightarrow 7\mathrm{Fe_3C} + 2\mathrm{C} \quad (4)$$

$$3\mathrm{Fe_2C} \rightarrow 2\mathrm{Fe_3C} + \mathrm{C} \quad (5)$$

The cementite is further decomposed into metallic iron and graphite. The quantitative analysis of the XRD pattern (Table 3) and relative areas of the Mössbauer spectrum (Table 4) of the PB3 sample (the minor admixture of magnetite has been neglected) then gives an overall equation for the carbides decomposition:

$$3\mathrm{Fe_2C} + 1/7\mathrm{Fe_7C_3} + 32/7\mathrm{C} \rightarrow \mathrm{Fe_3C} + 4(\alpha,\gamma)-\mathrm{Fe} + 7\mathrm{C} \quad (6)$$

Conclusions

Thermally induced decomposition of an insoluble Prussian blue ($Fe_4[Fe(CN)_6]_3{\cdot}4H_2O$) under inert atmosphere consists of three main steps. After the dehydration, a restructuration of the original crystal lattice accompanied by the changes in valence and spin states of iron atoms and release of cyanogen—$(CN)_2$ take place. Above 400 °C, the decomposition of PB is finished resulting to iron carbides and graphite. The increase of temperature up to 1000 °C induces the formation of metallic iron, cementite and graphite. The overall decomposition reaction can be expressed by the following equation:

$$1000\,^{\circ}\mathrm{C}:\ \mathrm{Fe_4[Fe(CN)_6]_3\cdot 4H_2O} \rightarrow 4(\alpha,\gamma)-\mathrm{Fe} + \mathrm{Fe_3C} + 7\mathrm{C} + 5(\mathrm{CN})_2 + 4\mathrm{N_2} + 4\mathrm{H_2O} \quad (7)$$

More detailed characterization of the ferrocyanide intermediate, which was found to be unstable in an opened air, is a subject of future investigations.

Acknowledgements This study has been supported by the Operational Program Research and Development for Innovations—European Regional Development Fund (CZ.1.05/2.1.00/03.0058), the internal IGA grants of Palacky University (PrF_2010_010, PrF_2011_013), the projects of the Ministry of Education of the Czech Republic (1M6198959201 and MSM6198959218), and the project of the Academy of Sciences of the Czech Republic (KAN115600801). The authors would like to thank to Jan Filip for XRD measurements, Martin Heřmánek for TG measurements, Jana Ševčíkova for Mössbauer measurements, Oldřich Schneeweiss for his comments on carbide phases, and Jiří Tuček for language corrections.

References

1. Buser HJ, Schwarzenbach D, Petter W, Ludi A. The crystal structure of Prussian blue: $Fe_4[Fe(CN)_6]_3 \cdot xH_2O$. Inorg Chem. 1977;163:2704–9.
2. Ito A, Suenaga M, Ono K. Mössbauer study of soluble Prussian blue, insoluble Prussian blue, and Turnbull's blue. J Chem Phys. 1968;48:3597–9.
3. Wilde RE, Ghosh SN, Marshall BJ. The Prussian blues. Inorg Chem. 1970;9:2512–6.
4. Weiser HB, Milligan WO, Bates JB. X-ray diffraction studies on heavy-metal iron-cyanides. J Phys Chem. 1942;46:99–111.
5. Allen JF, Bonnette AK. Thermal decomposition of Prussian blue: isotopic labeling with Mössbauer-inactive Fe-56. J Inorg Nucl Chem. 1974;36:1011–6.
6. Inoue H, Nakazawa T, Mitsuhashi T, Shirai T, Fluck E. Characterization of Prussian blue and its thermal decomposition products. Hyperfine Interact. 1989;46:725–31.
7. Ludi A, Güdel HU. Structural chemistry of polynuclear transition metal cyanides. Struct Bond. 1973;14:1–21.
8. Herren F, Fischer P, Ludi A, Hälg W. Neutron diffraction study of Prussian blue, $Fe_4[Fe(CN)_6]_3 \cdot xH_2O$. Location of water molecules and long-range magnetic order. Inorg Chem. 1980;19:956–9.
9. Vaucher S, Li M, Mann S. Synthesis of Prussian blue nanoparticles and nanocrystal superlattices in reverse microemulsions. Angew Chem Int Ed. 2000;39:1793–6.
10. Fiorito PA, Gonçales VR, Ponzio EA, Córdoba de Torresi SI. Synthesis, characterization and immobilization of Prussian blue nanoparticles. A potential tool for biosensing devices. Chem Commun. 2005;3:366–8.
11. Shen X, Wu S, Liu Y, Wang K, Xu Z, Lu W. Morphology synthesis and properties of well-defined Prussian blue nanocrystals by a facile solution approach. J Colloid Interface Sci. 2009;329:188–95.
12. Zhou PH, Xue DS. Finite-size effect on magnetic properties in Prussian blue nanowire arrays. J Appl Phys. 2004;96:610–4.
13. Karyakin AA, Karyakina EE. Electroanalytical applications of Prussian blue and its analogs. Russ Chem Bull Int Ed. 2001;50:1811–7.
14. Koncki R. Chemical sensors and biosensors based on Prussian blues. Crit Rev Anal Chem. 2002;32:79–96.
15. Puganova EA, Karyakin AA. New materials based on nanostructured Prussian blue for development of hydrogen peroxide sensors. Sensor Actuator B. 2005;109:167–70.
16. Rasmussen PG, Meyers EA. An investigation of Prussian blue analogues by Mössbauer spectroscopy and magnetic susceptibility. Polyhedron. 1984;3:183–90.
17. Verdaguer M, Girolami G. Magnetic Prussian blue analogs. In: Miller JS, Drillon M, editors. Magnetism: molecules to materials V. Weinheim: Wiley-VCH Verlag GmbH & Co. KGaA; 2005. p. 283–346.
18. Cosgrove JG, Collins RL, Murty DS. Preparation of ferrous ferricyanide (not Turnbull's blue). J Am Chem Soc. 1973;95:1083–6.
19. Zboril R, Machala L, Mashlan M, Sharma V. Iron(III) oxide nanoparticles in the thermally induced oxidative decomposition of Prussian blue, $Fe_4[Fe(CN)_6]_3$. Cryst Growth Des. 2004;4:1317–25.
20. De Marco D, Marchese A, Migliardo P, Bellomo A. Thermal analysis of some cyano compounds. J Therm Anal Calorim. 1987;32:927–37.
21. De Marco D. Thermal analysis of some cyano compounds. Part II. Thermal behaviour of mixed $KLnFe(CN)_6 \cdot 4H_2O$ (Ln = La(III), Ce(III), Nd(III)). Thermochim Acta. 1988;128:127–40.
22. De Marco D. Thermal analysis of some cyano compounds. Note III. The thermal behaviour of $Na_4Fe(CN)_6 \cdot 10H_2O$, $K_2Cu_3[Fe(CN)_6]_2 \cdot xH_2O$, $K_2Zn_3[Fe(CN)_6]_2 \cdot xH_2O$ and $Pb_2Fe(CN)_6$. J Therm Anal Calorim. 1989;35:2279–90.
23. De Marco D, Linert W. Thermal analysis of some cyano compounds. Part IV. The thermal behaviour of $LnFe^{3+}(CN)_6 \cdot nH_2O$ (La = La(III), Ce(III), Pr(III), Nd(III)). Thermochim Acta. 1991;175:249–61.
24. Brar AS, Sandhu HS, Sandhu SS. Thermal decomposition of hexahydrato thorium(IV) ferrocyanide. Thermochim Acta. 1980;41:253–6.
25. Lehto J, Haukka S, Koskinen P, Blomberg M. Thermal decomposition of potassium cobalt hexacyanoferrates(II). Thermochim Acta. 1990;160:343–7.
26. Navarro MC, Lagarrigue MC, De Paoli JM, Carbonio RE, Gómez MI. A new method of synthesis of BiFeO3 prepared by thermal decomposition of $Bi[Fe(CN)_6] \cdot 4H_2O$. J Therm Anal Calorim. 2010;102:655–60.
27. Gil DM, Navarro MC, Lagarrigue MC, Guimpel J, Carbonio RE, Gómez MI. Synthesis and structural characterization of perovskite YFeO3 by thermal decomposition of a cyano complex precursor, $Y[Fe(CN)_6] \cdot 4H_2O$. J Therm Anal Calorim. 2011;103:889–96.
28. Gallagher PK, Prescott B. Further studies of the thermal decomposition of europium hexacyanoferrate(III) and ammonium europium hexacyanoferrate(II). Inorg Chem. 1970;9:2510–2.
29. Žák T, Jirásková Y. CONFIT: Mössbauer spectra fitting program. Surf Interface Anal. 2006;38:710–4.
30. Nomura K, Takeda M, Iiyama T, Sakai H. Mössbauer studies of jarosite, mikasaite and Yapavaiite, and implication to their Martian counterparts. Hyperfine Interact. 2005;166:657–64.
31. Rodriguez-Carvajal J. An introduction to the program Fullprof 2000 (version July 2001). http://www.ill.eu/sites/fullprof/index.html.
32. Reguera E, Fernández-Bertrán J. Effect of the water of crystallization on the Mössbauer spectra of hexacyanoferrates (II and III). Hyperfine Interact. 1994;88:49–58.
33. Reguera E, Fernández-Bertrán J, Balmaseda J. The existence of ferrous ferricyanide. Transit Metal Chem. 1999;24:648–54.
34. Reguera E, Yee-Madeira H, Fernández-Bertran J, Nuñez L. Mössbauer spectra of ferrous salts of transition metal cyano complexes. A survey. Transit Metal Chem. 1999;24:163–7.
35. Herbstein FH, Snyman JA. Identification of Eckstrom-Adcock iron carbide as Fe_7C_3. Inorg Chem. 1964;3:894–6.
36. Lodya JAL, Gericke H, Ngubane J, Dlamini TH. Synthesis of Fe-carbides species by reactive milling. Hyperfine Interact. 2009;190:37–42.
37. Yamada Y, Yoshida H, Kouno K, Kobayashi Y. Iron carbide films produced by laser deposition. J Phys Conf Ser. 2010;217:012096.
38. Fang CM, van Huis MA, Zandbergen HW. Structure and stability of Fe_2C phases from density-functional theory calculations. Scr Mater. 2010;63:418–21.
39. Barton GH, Gale B. The Structure of a pseudo-hexagonal iron carbide. Acta Crystallogr. 1964;17:1460–2.

40. Niemantsverdriet JW, van der Kraan AM, van Dijk WL, van der Baan HS. Behavior of metallic iron catalysis during Fischer-Tropsch synthesis studied with Mössbauer spectroscopy, X-ray diffraction, carbon content determination, and reaction kinetic measurements. J Phys Chem. 1980;84:3363–70.
41. Amelse JA, Grynkewich G, Butt JB, Schwartz LH. Mössbauer spectroscopic study of passivated small particles of iron and iron carbide. J Phys Chem. 1981;85:2484–8.
42. Le Caër G, Dubois JM, Pijolar M, Perrichon V, Busslère P. Characterization by Mössbauer spectroscopy of iron carbides formed by Fischer-Tropsch synthesis. J Phys Chem. 1982;86: 4799–808.
43. Ron M. Iron-carbon and iron-nitrogen systems. In: Cohen RL, editor. Applications of Mössbauer spectroscopy, vol II. New York: Academic Press; 1980. p. 329–92.
44. Eckstrom HC, Adcock WC. A new iron carbide in hydrocarbon synthesis catalysis. J Am Chem Soc. 1950;72:1042–3.
45. Cohn EM, Hofer LJE. Mode of transition from Hägg iron carbide to cementite. J Am Chem Soc. 1950;72:4662–4.